Scattering by a Blade on a Metallic Plane

DANILO ERRICOLO
PIERGIORGIO L. E. USLENGHI
BADRIA ELNOUR
FRANCESCA MIOC

QUERY SHEET

QY: **Au: Please check all artwork throughout article for correctness. All images were obtained via electronic files supplied. Please ensure that there were no software interpretation problems.**

Q1: Au: Quality of Figure 1 artwork acceptable? If not, please supply better-quality image.

Q2: Au: Please check equation numbering from this point to the end of article. Some extra equation numbers appeared on the manuscript that did not pertain to any equation, so they were deleted. Please check all numbering in equations and in text as well for accuracy in cross referencing.

Q3: Au: Is this the same figure as Figure 1? Is this correct?

Electromagnetics, 26:000–000, 2006

ISSN: 0272-6343 print/1532-527X online
DOI: 10.1080/02726340500214910

Taylor & Francis
Taylor & Francis Group

Scattering by a Blade on a Metallic Plane

DANILO ERRICOLO
PIERGIORGIO L. E. USLENGHI
BADRIA ELNOUR

Department of Electrical and Computer Engineering
University of Illinois at Chicago
Chicago, Illinois USA

FRANCESCA MIOC

SATIMO
Roma, Italy

The scattering from a metal plane with a ridge is considered for the cases of plane wave and line source illumination and both polarizations. Exact analytical results are expressed using series that contain products of radial and angular Mathieu functions. The exact analytical results are computed and compared with high-frequency approximations and with measurements.

Keywords electromagnetic scattering, high-frequency scattering, Mathieu functions

Introduction

The diffraction of electromagnetic waves by an infinitely long metallic strip, or blade, of finite height connected to a metallic ground plane and perpendicular to it is considered. The primary source is a plane wave propagating in a direction perpendicular to the edge of the strip and polarized with its electric field either parallel (E polarization) or perpendicular (H polarization) to the edge, or an electric or magnetic line source parallel to the edge. The resulting two-dimensional boundary-value problem is solved exactly in terms of infinite series of products of radial and angular Mathieu functions. The total field is written as the sum of three terms: the incident field, the field that would be reflected by the metallic ground plane in the absence of the blade, and the scattered field due to the presence of the blade; this last contribution obeys the two-dimensional radiation condition and, for plane wave incidence, leads to an exact formula for the

Received 1 October 2004; accepted 30 May 2005.

This research was supported by the U.S. Department of Defense under MURI grant F49620-01-0436. The authors are thankful to the UIC Machine shop and Prof. Constantine Megaridis for providing some instrumentation needed for the measurements. Useful suggestions by the Reviewers are gratefully acknowledged.

Address correspondence to Danilo Erricolo, Department of Electrical and Computer Engineering, University of Illinois at Chicago, 851 South Morgan St., Chicago, IL 60607-7053, USA. E-mail: erricolo@ece.uic.edu

radar cross section of the blade. The geometry of the problem is presented in the next section, and the exact results for plane wave and line source incidence are reported in the following sections. A high-frequency solution is proposed; it is developed in detail for plane wave incidence. It consists of considering the edge of the blade as the edge of a half-plane on which two fields are incident: the primary wave, and its image in the ground plane. Each of these two waves is diffracted by the edge of the blade, and the diffracted field reaches the observation point both directly and after reflection from the ground plane. Thus, four separate diffraction mechanisms contribute to the scattered field at the observation point. For plane wave incidence, each mechanism consists of the sum of two terms, each the product of a Fresnel integral and an exponential. Since the blade is of finite height, some reflected-field terms must be subtracted, depending on the position of the observation point. This formulation takes into account the dihedral effect of the blade/ground-plane corner, but does not account for the multiple interactions between the blade's edge and the blade/ground-plane corner; thus, it is expected to become a better approximation as the ratio of blade height to wavelength increases. This high-frequency result is simplified for the far backscattered field and compared with the exact solution, whereas numerical results from the exact solutions are later compared to UTD results, for line source incidence. In the case of line source incidence, some bistatic results computed from the exact solutions for either polarization are also compared to measurements performed in an anechoic chamber. In all cases, previously known results are not repeated but may easily be found in the bibliography. In particular, a list of references on scattering by a strip may be found in Bowman, Senior, and Uslenghi (1987). The present work extends results presented by the authors (Uslenghi, Erricolo, & Mioc, 2000; Rahman et al., 2005). The frequency-domain analysis is conducted with a time-dependence factor $\exp(j\omega t)$, which is omitted throughout.

Geometry of the Problem

The cross section of the two-dimensional problem is shown in Figure 1. The axis $x = 0$ is a PEC plane and the blade OA is also a PEC. The points A and B are the foci of an elliptic coordinate system and their distance is the focal distance d. The relationship between elliptic cylinder and rectangular cartesian coordinates is

Figure 1

$$x = \frac{d}{2}\cosh u \cos v, \tag{1}$$

$$y = \frac{d}{2}\sinh u \sin v, \tag{2}$$

$$z = z, \tag{3}$$

where

$$0 \le u < \infty, \qquad 0 \le v \le 2\pi. \tag{4}$$

It is also convenient to introduce the variables (ξ, η, z) defined by

$$\xi = \cosh u, \qquad \eta = \cos v, \tag{5}$$

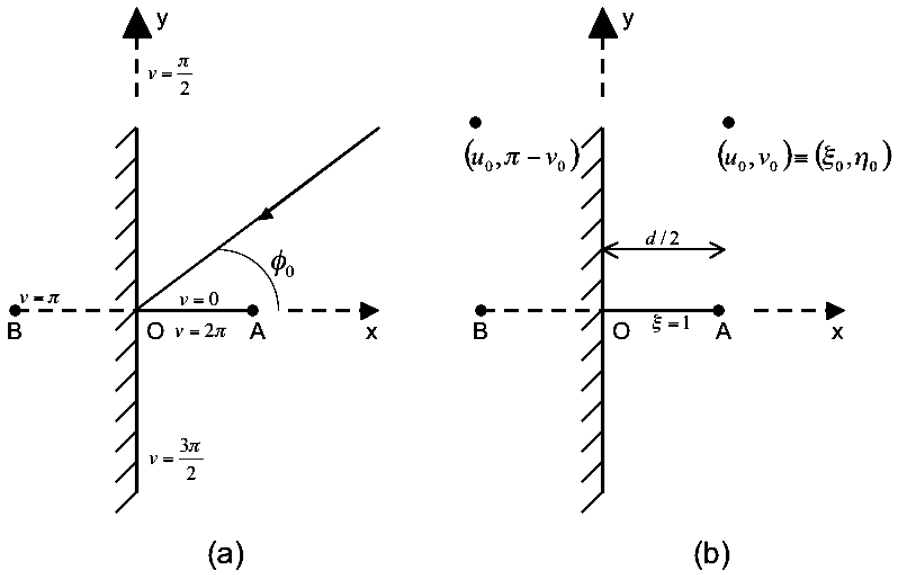

Figure 1. Geometry of the problem: (a) plane wave incidence, (b) line source incidence. **Q1**

where obviously $\xi \geq 1$ and $-1 \leq \eta \leq 1$. The coordinate surfaces with constant ξ are cylinders of elliptic cross section with foci at A and B. Coordinate surfaces with constant η are hyperbolas with the same foci. Observe that, if $\xi = 1$, each value of η defines a point (ξ, η) that falls on the segment of the x axis between the foci A and B. Similarly, if $\eta = 1(-1)$, each value of $\xi > 1$ defines a point on the segment of the x axis in the **65**
interval $x > d/2$ ($x < -d/2$). The positive portion of the y axis corresponds to $v = \pi/2$, and the negative portion, to $v = -\pi/2$. The formulas in subsequent sections contain the dimensionless quantity

$$c = k\frac{d}{2}, \tag{6}$$

where k is the wavenumber and d is the interfocal distance. The height of the blade $OA = d/2$. The inverse transformation from cartesian coordinates (x, y) to elliptic coordinates **70**
(ξ, η) is reported here for convenience:

$$\xi = \sqrt{\frac{4(x^2+y^2)+d^2+\sqrt{16(x^2+y^2)^2+d^4-8d^2(x^2-y^2)}}{2d^2}} \tag{7}$$

and

$$\eta = \frac{2x}{d\xi}. \tag{8}$$

The notation for the Mathieu functions that are used in the following sections is that of Stratton (1941).

Plane Wave Incidence

E Polarization

The incident field may be written as

$$E_z^i = \exp(jk(x\cos\varphi_0 + y\sin\varphi_0))$$
$$= \sqrt{8\pi}\sum_{m=0}^{\infty} j^m \left[\frac{1}{N_m^{(e)}}\mathrm{Re}_m^{(1)}(c,\xi)\mathrm{Se}_m(c,\eta)\mathrm{Se}_m(c,\cos\varphi_0) + \frac{1}{N_m^{(o)}}\mathrm{Ro}_m^{(1)}(c,\xi)\mathrm{So}_m(c,\eta)\mathrm{So}_m(c,\cos\varphi_0)\right]. \quad (9)$$

The total geometrical optics (incident plus reflected) field in the absence of the blade is

$$E_z^i + E_z^r = \sqrt{8\pi}\sum_{m=0}^{\infty} j^m \left[\frac{1-(-1)^m}{N_m^{(e)}}\mathrm{Re}_m^{(1)}(c,\xi)\mathrm{Se}_m(c,\eta)\mathrm{Se}_m(c,\cos\varphi_0) + \frac{1+(-1)^m}{N_m^{(o)}}\mathrm{Ro}_m^{(1)}(c,\xi)\mathrm{So}_m(c,\eta)\mathrm{So}_m(c,\cos\varphi_0)\right]. \quad (10)$$

The scattered field due to the presence of the blade that obeys the two-dimensional radiation condition is written as

$$E_z^s = \sqrt{8\pi}\sum_{m=0}^{\infty} j^m \left[\frac{a_m^{(e)}}{N_m^{(e)}}\mathrm{Re}_m^{(4)}(c,\xi)\mathrm{Se}_m(c,\eta)\mathrm{Se}_m(c,\cos\varphi 0) + \frac{a_m^{(o)}}{N_m^{(o)}}\mathrm{Ro}_m^{(4)}(c,\xi)\mathrm{So}_m(c,\eta)\mathrm{So}_m(c,\cos\varphi_0)\right]. \quad (11)$$

The modal coefficients $a_m^{(e)}$ and $a_m^{(o)}$ are obtained by applying the boundary conditions on the plane $x = 0$ and along the blade $\xi = 1$:

$$a_{2l}^{(e)} = a_{2l}^{(o)} = a_{2l+1}^{(o)} = 0, \quad (12)$$

$$a_{2l+1}^{(e)} = -2\frac{\mathrm{Re}_{2l+1}^{(1)}(c,1)}{\mathrm{Re}_{2l+1}^{(4)}(c,1)}. \quad (13)$$

Therefore, the perturbation field E_z^s is given by

$$E_z^s = -j2\sqrt{8\pi}\sum_{l=0}^{\infty}\frac{(-1)^l}{N_{2l+1}^{(e)}}\frac{\mathrm{Re}_{2l+1}^{(1)}(c,1)}{\mathrm{Re}_{2l+1}^{(4)}(c,1)} \times \mathrm{Re}_{2l+1}^{(4)}(c,\xi)\mathrm{Se}_{2l+1}(c,\eta)\mathrm{Se}_{2l+1}(c,\cos\varphi_0), \quad (14)$$

and the normalized bistatic cross section (see Uslenghi [2004]) is

$$\frac{\sigma_E(\varphi)}{\lambda} = 32\pi \left| \sum_{l=0}^{\infty} \frac{\mathrm{Re}_{2l+1}^{(1)}(c,1)}{N_{2l+1}^{(e)}\mathrm{Re}_{2l+1}^{(4)}(c,1)} \mathrm{Se}_{2l+1}(c,\cos\varphi_0)\mathrm{Se}_{2l+1}(c,\cos\varphi) \right|^2; \tag{15}$$

in particular, for backscattering ($\varphi = \varphi_0$): **85**

$$\frac{\sigma_E^{b.s.}(\varphi)}{\lambda} = 32\pi \left| \sum_{l=0}^{\infty} \frac{\mathrm{Re}_{2l+1}^{(1)}(c,1)}{N_{2l+1}^{(e)}\mathrm{Re}_{2l+1}^{(4)}(c,1)} (\mathrm{Se}_{2l+1}(c,\cos\varphi_0))^2 \right|^2. \tag{16}$$

H Polarization

The incident field is

$$\begin{aligned} H_z^i &= \exp(jk(x\cos\varphi_0 + y\sin\varphi_0)) \\ &= \sqrt{8\pi}\sum_{m=0}^{\infty} j^m \left[\frac{1}{N_m^{(e)}} \mathrm{Re}_m^{(1)}(c,\xi)\mathrm{Se}_m(c,\eta)\mathrm{Se}_m(c,\cos\varphi_0) \right. \\ &\qquad \left. + \frac{1}{N_m^{(o)}} \mathrm{Ro}_m^{(1)}(c,\xi)\mathrm{So}_m(c,\eta)\mathrm{So}_m(c,\cos\varphi_0) \right]. \end{aligned} \tag{17}$$

The total geometrical optics field (incident plus reflected) in the absence of the blade is

$$\begin{aligned} H_z^i + H_z^r = \sqrt{8\pi}\sum_{m=0}^{\infty} j^m \left[\frac{1+(-1)^m}{N_m^{(e)}} \mathrm{Re}_m^{(1)}(c,\xi)\mathrm{Se}_m(c,\eta)\mathrm{Se}_m(c,\cos\varphi_0) \right. \\ \left. + \frac{1-(-1)^m}{N_m^{(o)}} \mathrm{Ro}_m^{(1)}(c,\xi)\mathrm{So}_m(c,\eta)\mathrm{So}_m(c,\cos\varphi_0) \right]. \end{aligned} \tag{18}$$

The perturbation field due to the presence of the blade, which obeys the two-dimensional radiation condition, is written as **90**

$$\begin{aligned} H_z^s = \sqrt{8\pi}\sum_{m=0}^{\infty} j^m \left[\frac{b_m^{(e)}}{N_m^{(e)}} \mathrm{Re}_m^{(4)}(c,\xi)\mathrm{Se}_m(c,\eta)\mathrm{Se}_m(c,\cos\varphi_0) \right. \\ \left. + \frac{b_m^{(o)}}{N_m^{(o)}} \mathrm{Ro}_m^{(4)}(c,\xi)\mathrm{So}_m(c,\eta)\mathrm{So}_m(c,\cos\varphi_0) \right]. \end{aligned} \tag{19}$$

The modal coefficients $b_m^{(e)}$ and $b_m^{(o)}$ are obtained by applying the boundary conditions on the plane $x = 0$ and along the blade $\xi = 1$:

$$b_{2l}^{(e)} = b_{2l+1}^{(e)} = b_{2l}^{(e)} = 0, \tag{20}$$

$$b_{2l+1}^{(o)} = -2\frac{\mathrm{Ro}_{2l+1}^{(1)'}(c,1)}{\mathrm{Ro}_{2l+1}^{(4)'}(c,1)}. \tag{21}$$

Therefore, the perturbation field H_z^s is given by

$$H_z^s = -j2\sqrt{8\pi}\sum_{l=0}^{\infty}\frac{(-1)^l \mathrm{Ro}_{2l+1}^{(1)'}(c,1)}{N_{2l+1}^{(o)}\mathrm{Ro}_{2l+1}^{(4)'}(c,1)} \times \mathrm{Ro}_{2l+1}^{(4)}(c,\xi)\mathrm{So}_{2l+1}(c,\eta)\mathrm{So}_{2l+1}(c,\cos\varphi_0), \tag{22}$$

and the normalized bistatic cross section is given by

$$\frac{\sigma_H(\varphi)}{\lambda} = 32\pi\left|\sum_{l=0}^{\infty}\frac{\mathrm{Ro}_{2l+1}^{(1)'}(c,1)}{N_{2l+1}^{(o)}\mathrm{Ro}_{2l+1}^{(4)'}(c,1)}\mathrm{So}_{2l+1}(c,\cos\varphi_0)\mathrm{So}_{2l+1}(c,\cos\varphi)\right|^2; \tag{23}$$

in particular, for backscattering ($\varphi = \varphi_0$): **95**

$$\frac{\sigma_H^{b.s.}(\varphi)}{\lambda} = 32\pi\left|\sum_{l=0}^{\infty}\frac{\mathrm{Ro}_{2l+1}^{(1)'}(c,1)}{N_{2L+1}^{(o)}\mathrm{Ro}_{2l+1}^{(4)'}(c,1)}(\mathrm{So}_{2l+1}(c,\cos\varphi_0))^2\right|^2. \tag{24}$$

Line Source Incidence

E Polarization

Consider a line source parallel to the z-axis and located at the elliptic coordinates $(\xi_0, \eta_0) = (u_0, v_0) = (x_0, y_0)$, whose primary electric field is

$$\underline{E}^i = \hat{z}E_z^i = \hat{z}H_0^{(2)}(kR), \tag{25}$$

where **100**

$$R = \sqrt{(x-x_0)^2 + (y-y_0)^2} \tag{26}$$

is the distance between the line source and the observation point $(x, y) \equiv (u, v) \equiv (\xi, \eta)$. The incident field may be expanded in a series of elliptic cylinder functions (Bowman, Senior, & Uslenghi, 1987):

$$E_z^i = H_0^{(2)}(kr) = 4\sum_{m=0}^{\infty}\left[\frac{1}{N_m^{(e)}}\mathrm{Re}_m^{(1)}(c,\xi_<)\mathrm{Re}_m^{(4)}(c,\xi_>)\mathrm{Se}_m(c,\eta_0)\mathrm{Se}_m(c,\eta) + \frac{1}{N_m^{(o)}}\mathrm{Ro}_m^{(1)}(c,\xi_<)\mathrm{Ro}_m^{(4)}(c,\xi_>)\mathrm{So}_m(c,\eta_0)\mathrm{So}_m(c,\eta)\right], \tag{27}$$

where $\xi_<(\xi_>)$ means the smaller (larger) between ξ_o and ξ. Initially, one assumes that the ridge is absent so that the reflected field is given by an expression similar to (27), where **105** the image of the source is located at $(-x_0, y_0) \equiv (u_0, \pi - v_0)$, as shown in Figure 1.

The total geometrical optics (incident plus reflected) field is

$$E_z^i + E_z^r = 8\sum_{l=0}^{\infty}\left[\frac{\mathrm{Re}_{2l+1}^{(1)}(c,\xi_<)\mathrm{Re}_{2l+1}^{(4)}(c,\xi_>)}{N_{2l+1}^{(e)}}\mathrm{Se}_{2l+1}(c,\eta_0)\mathrm{Se}_{2l+1}(c,\eta)\right.$$
$$\left. + \frac{\mathrm{Ro}_{2l}^{(1)}(c,\xi_<)\mathrm{Ro}_{2l}^{(4)}(c,\xi_>)}{N_{2l}^{(o)}}\mathrm{So}_{2l}(c,\eta_0)\mathrm{So}_{2l}(c,\eta)\right]. \tag{28}$$

With the ridge present, the total field is given by

$$E_z = E_z^i + E_z^r + E_z^s, \tag{29}$$

where the scattered field E_z^s represents a perturbation to the geometrical optics field (28) and is written as

$$E_z^s = 8\sum_{l=0}^{\infty}\left[\frac{A_{2l+1}^{(e)}}{N_{2l+1}^{(e)}}\mathrm{Re}_{2l+1}^{(4)}(c,\xi)\mathrm{Se}_{2l+1}(c,\eta_0)\mathrm{Se}_{2l+1}(c,\eta)\right.$$
$$\left. + \frac{A_{2l}^{(o)}}{N_m^{(o)}}\mathrm{Ro}_{2l}^{(4)}(c,\xi)\mathrm{So}_{2l}(c,\eta_0)\mathrm{So}_{2l}(c,\eta)\right]. \tag{30}$$

The modal coefficients $A_{2l+1}^{(e)}$ and $A_{2l}^{(o)}$ are obtained by applying the boundary conditions along the metal surfaces using the properties reported in Uslenghi (2004) and Erricolo and Uslenghi (2004), which yield

$$A_{2l+1}^{(e)} = -\frac{\mathrm{Re}_{2l+1}^{(1)}(c,1)\mathrm{Re}_{2l+1}^{(4)}(c,\xi_0)}{\mathrm{Re}_{2l+1}^{(4)}(c,1)}, \tag{31}$$

$$A_{2l}^{(o)} = 0. \tag{32}$$

H Polarization

The incident field is given by

$$H_z^i = H_0^{(2)}(kr) = \sum_{m=0}^{\infty}\left[\frac{1}{N_m^{(e)}}\mathrm{Re}_m^{(1)}(c,\xi_<)\mathrm{Re}_m^{(4)}(c,\xi_>)\mathrm{Se}_m(c,\eta_0)\mathrm{Se}_m(c,\eta)\right.$$
$$\left. + \frac{1}{N_m^{(o)}}\mathrm{Ro}_m^{(1)}(c,\xi_<)\mathrm{Ro}_m^{(4)}(c,\xi_>)\mathrm{So}_m(c,\eta_0)\mathrm{So}_m(c,\eta)\right]. \tag{33}$$

Assuming that the ridge is absent, the application of the method of images yields the following expression for the total geometrical optics field:

$$H_z^i + H_z^r = 8\sum_{l=0}^{\infty}\left[\frac{\mathrm{Re}_{2l}^{(1)}(c,\xi_<)\mathrm{Re}_{2l}^{(4)}(c,\xi_>)}{N_{2l}^{(e)}}\mathrm{Se}_{2l}(c,\eta_0)\mathrm{Se}_{2l}(c,\eta)\right.$$
$$\left. + \frac{\mathrm{Ro}_{2l+1}^{(1)}(c,\xi_<)\mathrm{Ro}_{2l+1}^{(4)}(c,\xi_>)}{N_{2l+1}^{(o)}}\mathrm{So}_{2l+1}(c,\eta_0)\mathrm{So}_{2l+1}(c,\eta)\right]. \tag{34}$$

With the ridge present, the total field is given by

$$H_z = H_z^i + H_z^r + H_z^s, \tag{35}$$

where the scattered field H_z^s represents a perturbation to the geometrical optics field (34) and is written as

$$H_z^s = 8\sum_{l=0}^{\infty}\left[\frac{B_{2l}^{(e)}}{N_{2l}^{(e)}}\mathrm{Re}_{2l}^{(4)}(c,\xi)\mathrm{Se}_{2l}(c,\eta_0)\mathrm{Se}_{2l}(c,\eta) + \frac{B_{2l+1}^{(o)}}{N_{2l+1}^{(o)}}\mathrm{Ro}_{2l+1}^{(4)}(c,\xi)\mathrm{So}_{2l+1}(c,\eta_0)\mathrm{So}_{2l+1}(c,\eta)\right]. \tag{36}$$

The application of the boundary conditions leads to

$$B_{2l}^{(e)} = 0, \tag{37}$$

$$B_{2l+1}^{(o)} = -\frac{\mathrm{Ro}_{2l+1}^{(1)'}(c,1)\mathrm{Ro}_{2l+1}^{(4)}(c,\xi_0)}{\mathrm{Ro}_{2l+1}^{(4)'}(c,1)} \tag{38}$$

Comparison with High-Frequency Approximations

The exact results derived in the previous sections are evaluated using subroutines described in Zhang and Jin (1996) and the acceleration technique presented in Erricolo (2003).

A high-frequency approximation for the field scattered by the blade in the presence of the ground plane is obtained assuming that the ground plane is removed, thus leaving the strip AB shown in Figure 1. The total field is computed considering the incident field, its image with respect to the initial location of the ground plane, and the single diffraction contributions from the edges of the strip. The diffraction by each edge is evaluated by taking the exact scattering by a PEC half-plane and then inserting the asymptotic approximations for the Fresnel integrals. As such, it is a first-order high-frequency result that does not take into account the interaction between the edges. Hence, the approximated expression for the backscattered electric field is

$$E_z^{b.s.} \approx \frac{\exp(-jk\rho + j\pi/4)}{\sqrt{2\pi k\rho}}\{\exp(-j2c\cos\varphi_0)[2c\sin\varphi_0 + C_E(c,\varphi_0)]\}, \tag{39}$$

where

$$C_E(c,\varphi_0) = j\cos(2c\cos\varphi_0) - \left[\frac{\sin(2c\cos\varphi_0)}{\cos\varphi_0} + \frac{j}{\sin\varphi_0}\right]. \tag{40}$$

The approximated monostatic radar cross section is

$$\frac{\sigma_E^{b.s.}}{\lambda} = \frac{1}{2\pi}|2c\sin\varphi_0 + C_E(c,\varphi_0)|^2. \tag{41}$$

Figure 2 shows the comparison between the exact result given in (16) and the high-frequency result given in (41). Only values of φ_0 that satisfy $10^0 < \varphi_0 < 80^0$ are considered because the approximation (41) requires **Figure 2**

$$\sqrt{2k\rho}\begin{Bmatrix}\sin\\ \cos\end{Bmatrix}\varphi_0 \gg 1, \tag{42}$$

$\sqrt{2k\rho}\sin\varphi_0 \gg 1$. One observes that for small values of c the difference between the two curves is as large as approximately 15 dB, while the agreement significantly improves for larger values of c. **140**

It is also possible to obtain an approximated expression in the case of H polarization. The result for the backscattered magnetic field is

$$H_z^{b.s.} \approx \frac{\exp(-jk\rho + j\pi/4)}{\sqrt{2\pi k\rho}}\{\exp(-j2c\cos\varphi_0)[2c\sin\varphi_0 + C_H(c,\varphi_0)\}, \tag{43}$$

where **145**

$$C_H(c,\varphi_0) = j\cos(2c\cos\varphi_0) + \left[\frac{\sin(2c\cos\varphi_0)}{\cos\varphi_0} + \frac{j}{\sin\varphi_0}\right]. \tag{44}$$

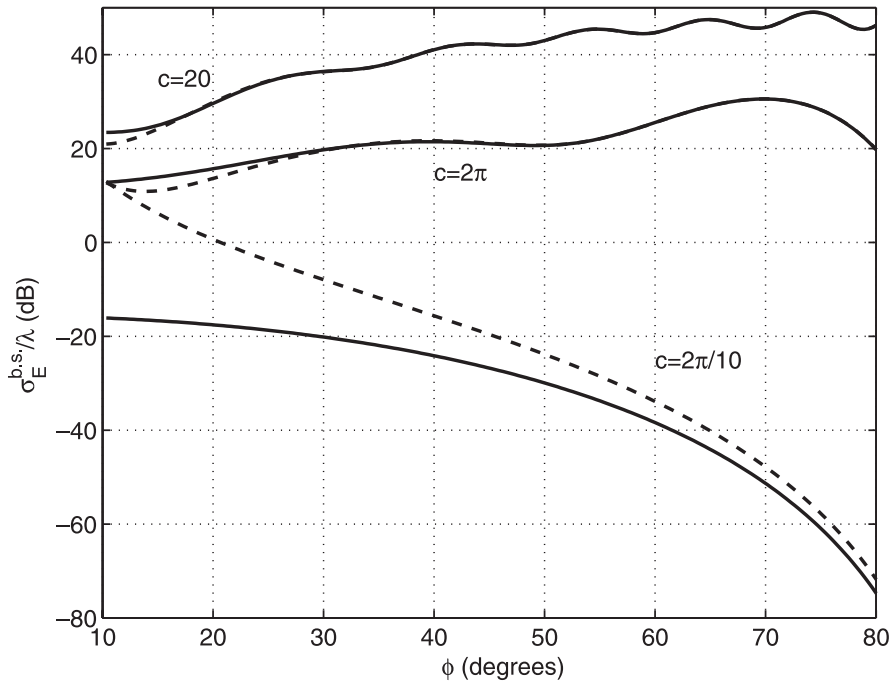

Figure 2. Comparison of the monostatic RCS, in dB, computed using the exact analytical formula (16) and the high-frequency approximation (41) for an E-polarized incident plane wave. The solid lines correspond to the exact solution, while the dashed lines represent the high-frequency approximation.

The approximated monostatic radar cross section is

$$\frac{\sigma_H^{b.s.}}{\lambda} = \frac{1}{2\pi}|2c\sin\varphi_0 + C_H(c,\varphi_0)|^2. \tag{45}$$

Figure 3 shows the comparison between the exact result (24) and the approximate result (45). In the case of H polarization, the discrepancy between the approximated (45) and exact (24) results is larger than for the corresponding values of c in the case of E polarization. This may be due to a traveling wave between the edges that is present for H polarization but not for E polarization. However, as expected, the agreement improves for larger values of c.

Figure 3

150

Comparison with the Uniform Theory of Diffraction

The exact total fields given by (29) and (35) for the E and H polarizations, respectively, are approximated using the uniform theory of diffraction (UTD) (Kouyoumjan & Pathak, 1974; Balanis, 1989). Similar to the high-frequency approximation of the previous section, the UTD approximation is obtained by removing the metal plane $x = 0$, introducing the image OB of the segment OA and the image of the source. As a result, the contribution of the source towards the observation point will consist of two diffracted rays and, if a

155

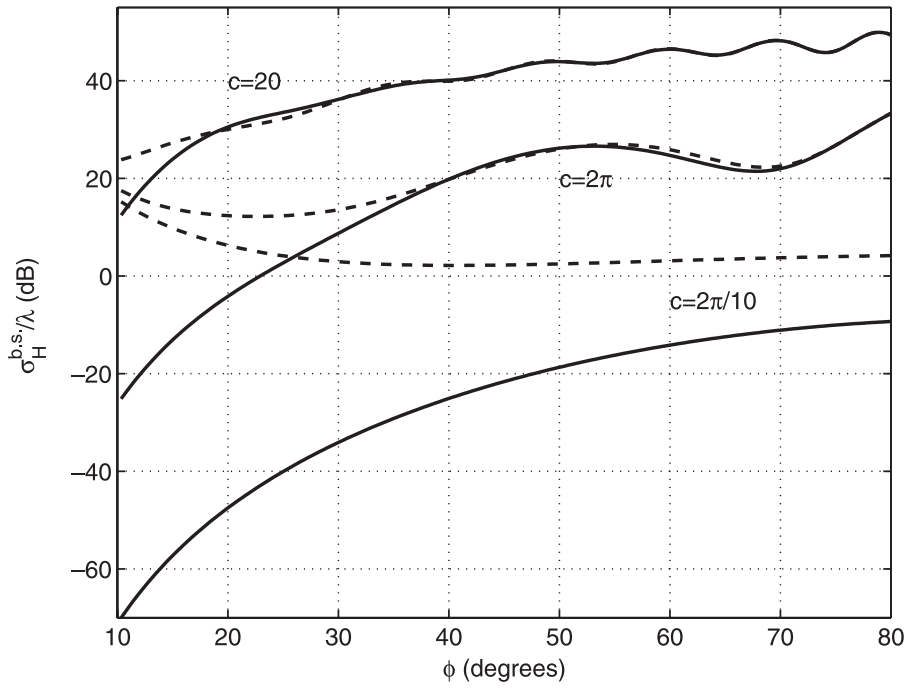

Figure 3. Comparison of the monostatic RCS, in dB, computed using the exact analytical formula (24) and the high-frequency approximation (45) for an H-polarized incident plane wave. The solid lines correspond to the exact solution, while the dashed lines represent the high-frequency approximation.

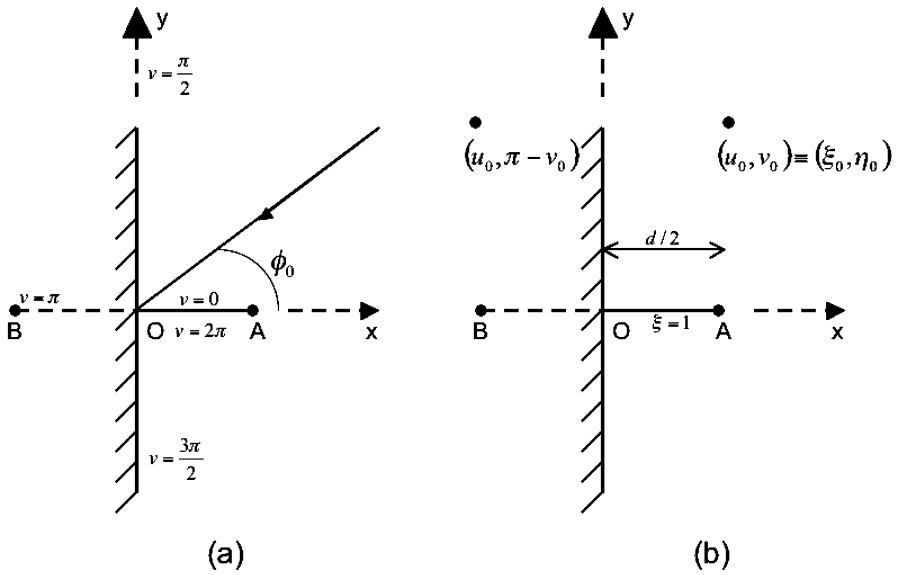

Figure 4. Geometry of the problem without the PEC plane. This figure only shows the contribution from the original source, but another set of three rays needs to be considered to account for the total field. **Q3**

line of sight exists, a direct ray, as shown in Figure 4. A similar set of rays must also be considered for the image of the source. **Figure 4**

Figure 5 shows the results for the comparison when the incidence is an E-polarized plane wave. The curves for the exact and UTD results overlap for the values considered for c along the observation segment that is located close to the blade at a distance of only one wavelength; in fact, a small difference is noticeable only when c is quite small, as in Figure 5a. **Figure 5**

Figure 6 shows the results for line source incidence and E polarization. In all three cases, the agreement between the exact theory and the high-frequency method is very good. In fact, one can hardly recognize that for each value of c two curves are actually overlapped, even though the distances among source, ridge, and observation point are only a few wavelengths. **Figure 6**

Figure 7 shows the results for line source incidence and H polarization. Unlike the case of E polarization, it is possible to observe the difference between the solid and dashed line. This difference is particularly noticeable for the case $c = 1$, which corresponds to a ridge that is shorter than one wavelength. When the value of c increases, the UTD approximation provides results that are closer to the exact ones. **Figure 7**

Comparison with Measurements

Experiments were also conducted to compare the theoretical results given by (29) and (35) with measurements. The measurements were taken in the anechoic room at the University of Illinois at Chicago and the antennas used in the experiments were the same

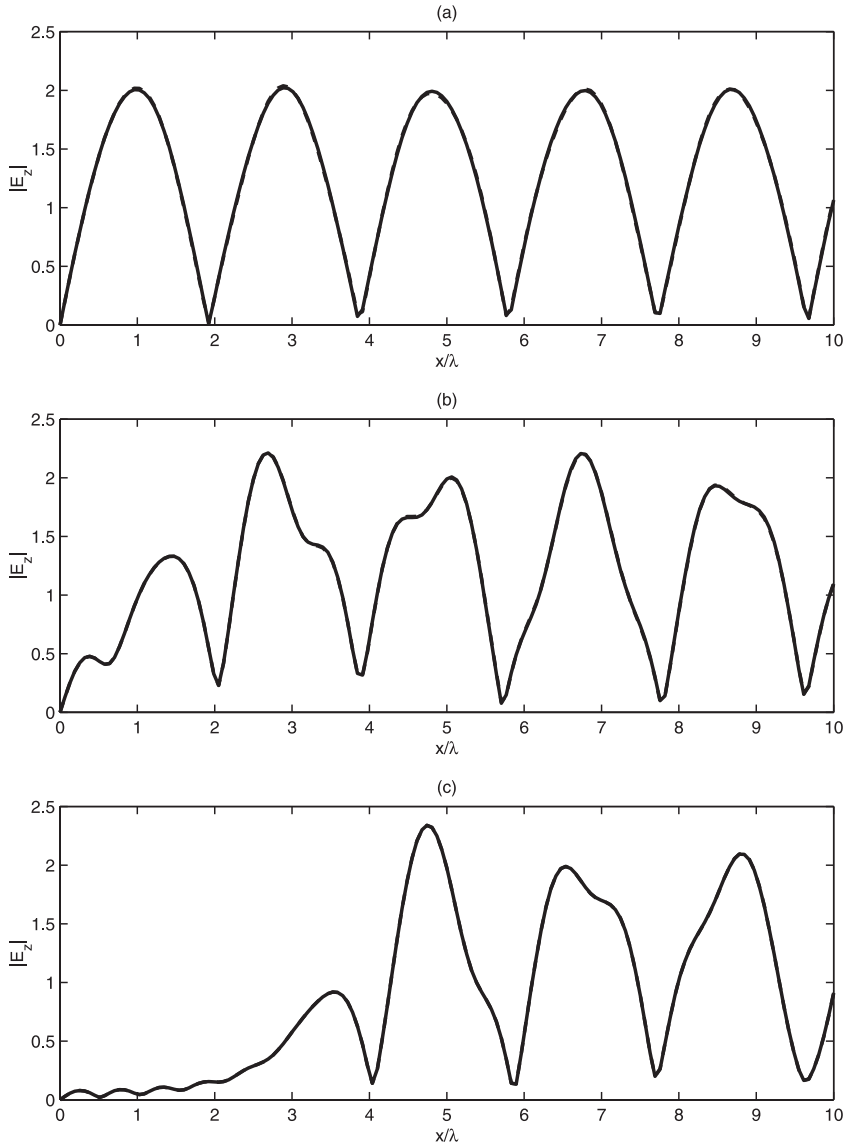

Figure 5. E-polarized plane wave incident at an angle $\varphi_0 = 75^0$. The total normalized field $|E_z|$ is computed along the line ($0 \leq x \leq 10\lambda$, $y = -\lambda$). The results correspond to: (a) $c = 2\pi/10$; (b) $c = 2\pi$; and $c = 20$.

used for the experiments described in Erricolo, D'Elia, and Uslenghi (2002) and Erricolo, Crovella, and Uslenghi (2002). Figure 8 shows the results for the E-polarization case. One can observe a very good agreement when the distance of the observation point from the ground plane exceeds approximately 12λ. When the observation point is closer to the the ground plane the agreement is not so good and this behavior is attributed to an interaction between the antenna used in the experiment and the metallic plane. Similar observations apply to Figure 9.

180 **Figure 8**

185 **Figure 9**

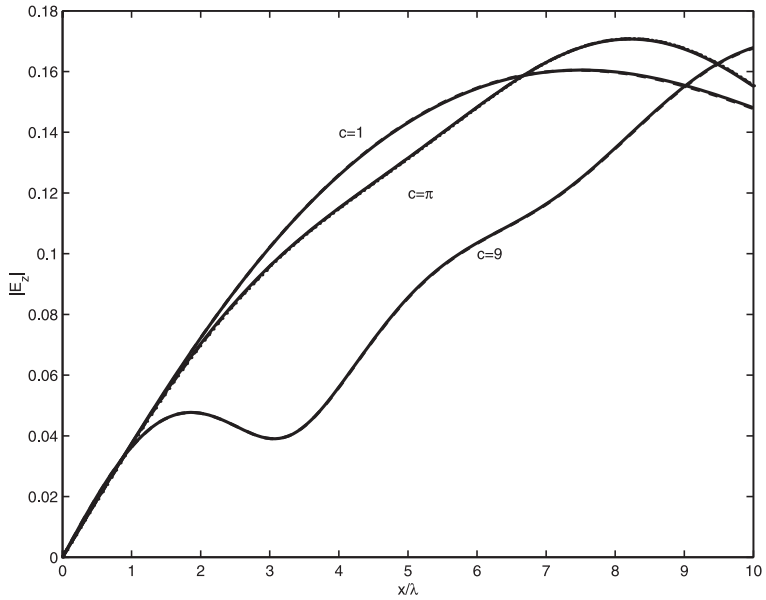

Figure 6. E polarization. Total normalized field $|E_z|$ due to a line source located at ($x_0 = \lambda/2$, $y_0 = 4\lambda$) when the observation point moves along the line ($0 \leq x \leq 10\lambda$, $y = -10\lambda$). The solid lines represent the exact results, while the dashed lines represent the UTD approximation. Because of the close agreement between the exact results and the UTD approximation, the two sets of curves overlap very well and it is hardly noticeable any difference. The computed results correspond to: (1) $c = 1$; (2) $c = \pi$; and (3) $c = 9$.

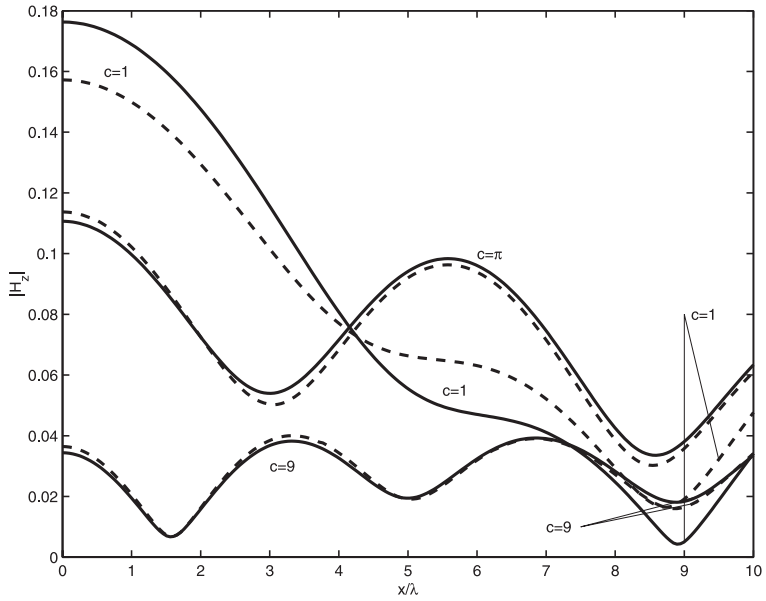

Figure 7. H polarization. Total normalized field H_z due to a line source located at ($x_0 = \lambda/2$, $y_0 = 4\lambda$) when the observation point moves along the line ($0 \leq x \leq 10\lambda$, $y = -10\lambda$). The solid lines represent the exact results, while the dashed lines represent the UTD approximation. The computed results correspond to: (1) $c = 1$; (2) $c = \pi$; and (3) $c = 9$.

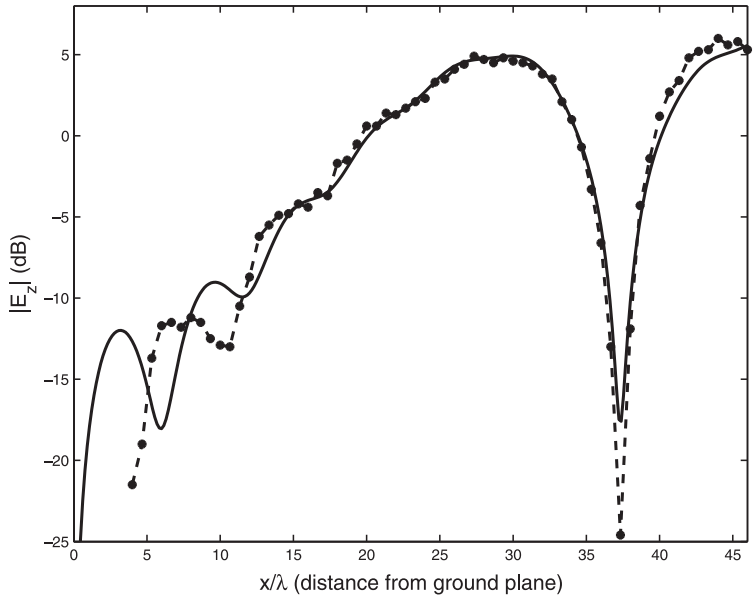

Figure 8. E polarization. Normalized value of the total field $|E_z|$ due to a line source located at ($x_0 = 6.25\lambda$, $y_0 = 115\lambda$) when the observation point moves along the line ($0 \leq x \leq 46\lambda$, $y = -114.17\lambda$). The solid line represents the exact results, while the dashed line represents the measurements. These results correspond to $c = 52$.

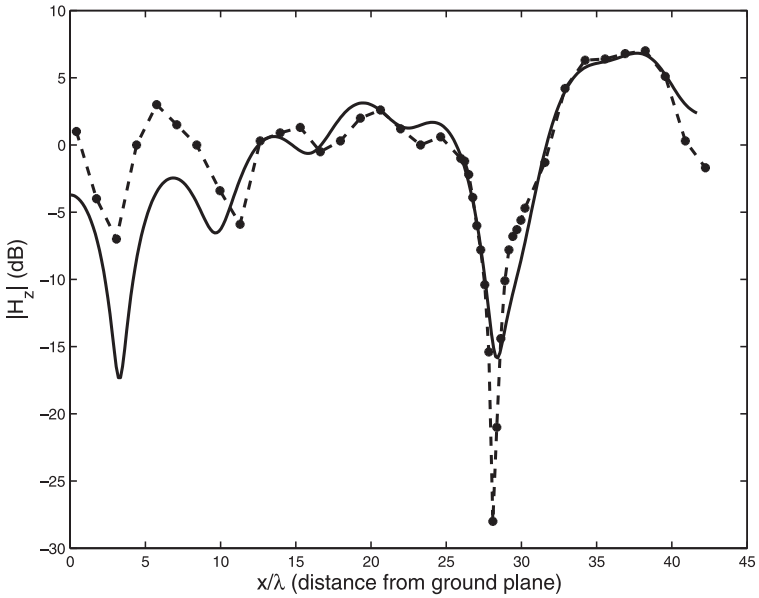

Figure 9. H polarization. Normalized value of the total field $|H_z|$ due to a line source located at ($x_0 = 6.25\lambda$, $y_0 = 115\lambda$) when the observation point moves along the line ($0 \leq x \leq 42\lambda$, $y = -114.17\lambda$). The solid line represents the exact results, while the dashed lines represent the measurements. These results correspond to $c = 52$.

Conclusion

The results obtained in this work are important because they present exact solutions to a new boundary value problem, thus enriching the list of geometries for known canonical solutions. Other exact solutions to new boundary value problems have been presented in Uslenghi (2004) and Erricolo and Uslenghi (2004). Additionally, the comparisons with high-frequency approximations and measurements confirm the validity of the theoretical predictions. We could have introduced higher order terms in the high-frequency approximations; however, we wanted to show that the first-order terms can provide accurate results, even with relatively small values of c.

It should be noted that the results obtained in this work can also be derived from the results for a PEC strip, in free space, by utilizing the method of images.

References

Balanis, C. A. 1989. *Advanced engineering electromagnetics*, New York: Wiley.

Bowman, J. J., T. B. A. Senior, & P. L. E. Uslenghi. 1987. *Electromagnetic and acoustic scattering by simple shapes*. New York: Hemisphere Publishing.

Erricolo, D. 2003. Acceleration of the convergence of series containing Mathieu functions using Shanks transformation. *IEEE Antennas Wireless Propagat. Lett*. 2:58–61.

Erricolo, D., U. G. Crovella, & P. L. E. Uslenghi. 2002. Time-domain analysis of measurements on scaled urban models with comparisons to ray-tracing propagation simulation. *IEEE Trans. Antennas Propagat.* 50(5):736–741.

Erricolo, D., G. D'Elia, & P. L. E. Uslenghi. 2002. Measurements on scaled models of urban environments and comparisons with ray-tracing propagation simulation. *IEEE Trans. Antennas Propagat.* 50(5):727–735.

Erricolo, D., & P. L. E. Uslenghi. 2004. Exact radiation and scattering for an elliptic metal cylinder at the interface between isorefractive half-spaces. *IEEE Trans. Antennas Propagat.* 52(9):2214–2225.

Kouyoumjian, R. G., & P. H. Pathak. 1974. A uniform geometrical theory of diffraction for an edge in a perfectly conducting surface. *Proc. IEEE* 62(11):1448–1461.

Rahman, S., B. Elnour, D. Erricolo, & P. L. E. Uslenghi. 2005. Measurements and theoretical results for the scattering by a ridge on a metal plane. In *Digest of National Radio Science Meeting*, Boulder, CO, p. 86.

Stratton, J. A. 1941. *Electromagnetic theory*. New York: McGraw-Hill.

Uslenghi, P. L. E. 2004. Exact penetration, radiation and scattering for a slotted semielliptical channel filled with isorefractive material. *IEEE Trans. Antennas Propagat.* 52(6):1473–1480.

Uslenghi, P. L. E., D. Erricolo, & F. Mioc. 2000. Exact scattering by a ridge on a metal plane with isorefractive quadrants. In *Digest of National Radio Science Meeting*, Salt Lake City, Utah, p. 141.

Zhang, S., & J.-M. Jin. 1996. *Computation of special functions*. New York: Wiley.